Low-Order Modeling to Investigate Clusters of Intrinsic Thermoacoustic Modes in Annular Combustors

Guillaume J. J. Fournier*
Technical University of Munich
Department of Mechanical Engineering
D-85747 Garching, Germany
e-mail: fournier@tfd.mw.tum.de

Matthias Haeringer
Technical University of Munich
Department of Mechanical Engineering
D-85747 Garching, Germany
e-mail: haeringer@tfd.mw.tum.de

Camilo F. Silva
Technical University of Munich
Department of Mechanical Engineering
D-85747 Garching, Germany
e-mail: silva@tfd.mw.tum.de

Wolfgang Polifke
Technical University of Munich
Department of Mechanical Engineering
D-85747 Garching, Germany
e-mail: polifke@tum.de

ABSTRACT

The intrinsic thermoacoustic (ITA) feedbackloop constitutes a coupling between flow, flame and acoustics that does not involve the natural acoustic modes of the system. One recent study showed that ITA modes in annular combustors come in significant number and with the peculiar behavior of clusters, i.e. several modes with close frequencies. In the present work an analytical model of a typical annular combustor is derived via Riemann invariants and Bloch theory. The resulting formulation describes the full annular system as a longitudinal combustor with an outlet reflection coefficient that depends on frequency and the azimuthal mode order. The model explains the underlying mechanism of the clustering phenomena and the structure of the clusters associated with ITA modes of different azimuthal orders. In addition, a phasor analysis is proposed, which enclose the conditions for which the 1D model remains valid when describing the thermoacoustic behavior of an annular combustor.

NOMENCLATURE

S_b Cross section area of the burner tube

S_c Cross section area of the combustion chamber

α Cross section ratio between burner tube and chamber

m Bloch wave number

N Number of burners

p' Acoustic pressure

u' Acoustic velocity

c_u Speed of sound upstream the flame

c_d Speed of sound downstream the flame

ω Complex frequency

*Address all correspondence to this author.

L_b Length of the burner tubes

L Length between two burners

P_c Total length of the combustion chamber

FTF Flame Transfer Function

n Interaction index of the FTF

τ Time delay of the FTF

ξ Ratio of specific impedances

θ Normalized temperature ratio

$\dot{q}'$ Normalized global heat release fluctuations

$f,\ g$ Riemann invariants

He Helmholtz number

$\mathscr{R}_m$ Equivalent reflection coefficient

$\mathscr{L}_m$ Effective length

INTRODUCTION

To tackle environmental issues and reduce emissions, in particular NO_x pollutants, lean premixed combustion systems have been developed. However this combustion technology is more prone to thermoacoustic combustion instabilities [1, 2]. This type of self-excited instability results from coupling between the unsteady heat release of the flame and acoustic waves, which may result in a positive feedback loop, thus inducing growing pressure fluctuations. Repeated exposure to high pressure levels over time will promote mechanical fatigue and may lead to catastrophic failure of the combustor [3]. From a safety perspective, it is crucial to identify the important flow-flame-acoustic interaction and feedback mechanisms in order to prevent this type of instability.

Bomberg et al. [4] identified the so-called intrinsic thermoacoustic (ITA) feedback loop, which does not involve reflection of acoustic waves at the combustor inlet or exit. Instead, the ITA feedback mechanism may be described as follows: velocity sensitive flames respond to a perturbation of upstream velocity with a change in the heat release rate, which in turn generates acoustic waves that travel in both up- and downstream directions. The wave traveling in the upstream direction will directly perturb the acoustic velocity, before even reaching the boundaries of the acoustic system. This mechanism of flow-flame-acoustic interaction is, in a sense, *intrinsic* to the flame and its immediate surrounding, hence its name.

Anomalous peaks in the acoustic flame response, i.e. the magnitude of coefficients of the flame scattering matrix [5], and in the so-called instability potentiality [6] were explained as resonances of the ITA feedback loop [4, 7].

Furthermore, ITA feedback provided an explanation [7] of the physical nature of thermoacoustic instabilities of a flame in an anechoic environment, which were reported and analyzed by Hoeijmakers et al. [8, 9] and subsequently confirmed by high-fidelity CFD simulations with non-reflecting boundary conditions [10, 11]. Emmert et al. [12] then argued that ITA feedback gives rise to additional thermoacoustic modes that are not related to acoustic eigenmodes of the combustor, and identified such an "ITA mode" as the dominant unstable eigenmode in a premix swirl combustion test rig. This constitutes a significant deviation from the established interpretation of thermoacoustic instabilities as acoustic eigenmodes of the combustor driven by unsteady heat release [13].

The concept of ITA feedback can explain in hindsight a number of hitherto inexplicable phenomena described in earlier studies. For example, the "new set of modes associated with flame model" described by Dowling and Stow [14] quite obviously should be considered as "modes of ITA origin" [15]. Similarly, there is strong evidence that the low frequency "bulk mode" discussed by Eckstein and Sattelmayer [16] results from ITA feedback [17]. Finally, "convective scaling" of thermoacoustic eigenfrequencies – i.e. the dependence of eigenmode frequency on the bulk flow velocity inside the burner, but not on the speed of sound in plenum or combustor – may be regarded as a consequence of ITA feedback [18].

Hosseini et al. [19] investigated the interplay between thermoacoustic modes of ITA and acoustic origin and showed that when the passive acoustic mode is far away from the ITA, the two do not interplay with each other. More recently, Sogaro et al. [20] investigated a pairwise interplay between acoustic and ITA modes and showed that modal sensitivities increase as the two modes approach each other. Silva et al. [21] and Orchini et al. [22] further investigated ITA and acoustic modes and their interplay with exceptional points. They demonstrated that away from the exceptional point and the acoustic mode, the ITA trajectories when varying the gain and time delay of the flame are straight lines, i.e. their growth rate changes but the frequency remains approximately constant.

Previous studies [7, 9, 15] showed analytically that eigenfrequencies of ITA modes in a one-dimensional Rijke tubes with anechoic boundary conditions have solution in the form

$$\omega = \frac{\pi(2j+1)}{\tau} - \frac{i}{\tau}\ln\left(\frac{n\theta}{1+\xi}\right), \quad j \in \mathbb{N} \tag{1}$$

where $\xi = \frac{\rho_u c_u}{\rho_d c_d}$ is the ratio of specific impedances upstream and downstream the flame, n and τ the gain and time delay associated to the flame response, respectively and $\theta = (T_d - T_u)/T_u$ the normalized temperature ratio. In the rest of the present paper, we will refer to Eqn. (1), the frequency of the ITA mode in an anechoic environment, as the pure ITA frequency. Mukherjee and Shrira [15] showed that, for a Rijke tube with fully reflecting boundaries, in the limit

of small n, the ITA mode is highly damped but its frequency remains close to a corresponding "pure ITA frequency".

Buschmann et al. [23, 24] and Orchini et al. [22] observed the existence of ITA modes in annular combustors. These modes come in significant number and have the peculiar behavior of appearing in clusters, i.e. several modes with different growth rate, but very close frequencies. So far, little has been done to explain their origin. Recall at this point Emmert et al. [12], who demonstrated that in longitudinal combustors with partially reflecting boundaries ITA modes should not be ignored and indeed can be the most unstable modes. Furthermore, the analysis suggested that established methods for passive control (dampers, etc.) have little influence on ITA modes, or worse, can lead to the opposite effect and trigger an instability. Therefore, it is crucial to understand the underlying physics behind ITA modes. The goal of the present study is to investigate ITA modes in annular chambers.

Various tools are available to study thermoacoustic instabilities: high-fidelity LES simulations [25,26], Linearized Reactive Flow [27], Linearized Navier-Stokes equations [28, 29] give excellent results, but at considerable computational cost. Helmholtz solvers [30] are more affordable and able to accurately model complex 3D geometries, but computational cost remains non negligible. On the other hand, low-order network models [31–35] applied for annular geometries have proven to give satisfactory agreement at extremely low computational cost. Bloch theory [36], which exploits the rotational symmetry of a system, has recently been applied in the thermoacoustic community [22, 37–39]. This approach reduces a system with rotational symmetries to a single unit cell and facilitates its computation without loss in accuracy.

In the present study, we propose a low-order network model formulated with Bloch boundary conditions to investigate ITA modes in an annular combustor. The paper is structured as follows: we first describe the network model with Bloch boundary conditions that represents the combustor. We then derive an analytical expression of the equivalent reflection coefficient that models the chamber behavior and demonstrate that the system can be reduced to a simple longitudinal set-up. This reduced model is applied to a typical lab-scale combustor to explain the origin of ITA clusters. It also enables us to explain the spectrum of the combustor and the damping of modes with higher azimuthal order. We then give explanations on the shift of certain modes and the offset from their respective clusters.

NETWORK MODEL OF AN ANNULAR GEOMETRY WITH BLOCH BOUNDARY CONDITIONS

Case and Flow Description

The combustor consists of N perfectly premixed burners connected to an annular combustion chamber. For the sake of simplicity, the plenum is not taken into account, because it can often be decoupled [40, 41]. The area ratio between plenum and burners is assumed large enough such that the burners can be modeled by ducts terminating in a large vessel. For low Mach numbers, this leads to a reflection coefficient at the inlet of the burners of $R_{\text{in}} = -1$. At the

exit of a gas turbine combustion chamber, a high pressure turbine stage is placed in order to extract energy from the fluid and transform it into mechanical work. Marble and Candel [42] showed that the acoustic response of the turbine inlet can be modeled with a fixed gain lower than 1 and a zero phase response. To simplify the study, we choose here a reflection of $R_{\text{out}} = 1$ and we expect little quantitative change when accounting for the losses [43]. In this study, we also neglect entropy waves, assuming they play a negligible role [44].

The model is based on a network approach. The burners and the combustion chamber are modeled by ducts where only 1D planar acoustic waves propagates. In the chamber, only purely azimuthal modes are considered. The axial length of the chamber is assumed to be small compared to the azimuthal length P_c; mixed modes will occur at higher frequencies and are not considered here. Transverse modes are also out of the scope of this study. The chamber is decomposed into N ducts of length L, where L is the distance between two burners. Similarly to Parmentier et al. [33], burners and chamber are connected with T-junctions and the flames are placed inside the burners, just before the area change with the chamber. The flames and the T-junctions are assumed to be acoustically compact.

Flame and Unsteady Heat Release Model

The acoustic flame model is based on linearized Rankine Hugoniot jump equations across a compact heat source [7, 45] with heat release fluctuations.

$$\begin{cases} \dfrac{p'_d}{\bar{\rho}_d c_d} = \xi \dfrac{p'_u}{\bar{\rho}_u c_u} \\ u'_d = u'_u + \theta \dot{q}' \end{cases} \tag{2}$$

where $\xi = \bar{\rho}_u c_u / \bar{\rho}_d c_d$ is the ratio of specific impedances, $\theta = (T_d - T_u)/T_u$ the normalized temperature ratio and $\dot{q}' = \dot{Q}' \bar{u}_u / \bar{\dot{Q}}$ the normalized global heat release fluctuations of the flame.

The model is closed by a Flame Transfer Function (FTF) which relates upstream velocity fluctuations at the reference position with the normalized global heat release fluctuations of the flame. Crocco [46] introduced a simple model with only 2 parameters, a gain n and a time delay τ, which represent the delay between the acoustic perturbation and the actual response of the flame.

$$\frac{\dot{q}'}{u'_u} = \mathscr{F}(\omega) = n e^{-i\omega\tau} \tag{3}$$

This model is simplistic but captures essential aspects of a generic flame response and is convenient to use in the context of analytical models. Especially, the pure ITA frequency can be analytically expressed as recalled in Eqn. (1).

Bloch-Wave Theory

Bauerheim et al. [47] showed analytically that azimuthal modes are strongly influenced by symmetry breaking. Both geometrical or flow symmetry breaking cause the degenerate pairs of azimuthal modes to split into two distinct modes. In this study, the influence of symmetry breaking is not taken into account: the burners are identical and the chamber does not exhibit any mean flow in the azimuthal direction. Because of the discrete rotational symmetry, according to Bloch theory [36, 37], the acoustic pressure in the frequency domain can be written in the form:

$$\hat{p}(\boldsymbol{x}) = \psi(\boldsymbol{x})\, e^{im\theta}, \;\; m = \begin{cases} -\dfrac{N}{2}+1, \ldots, \dfrac{N}{2} & N \text{ even} \\ -\dfrac{N-1}{2}, \ldots, \dfrac{N-1}{2} & N \text{ odd} \end{cases} \tag{4}$$

where θ is the azimuthal coordinate around the axis of discrete rotational symmetry, $\psi(\boldsymbol{x})$ is a function identical in all unit cell and periodic in θ with a period $2\pi/N$ and m is the Bloch wave number. In this application, the absolute value of the Bloch wave number $|m|$ is identical to the azimuthal mode order because, in time domain, the solution $p(\boldsymbol{x},t) = \hat{p}(\boldsymbol{x})\, e^{i\omega t} = \psi(\boldsymbol{x})\, e^{i(\omega t + m\theta)}$ is a traveling wave in the azimuthal coordinate θ [38].

Depending on the values of m, the modes can be classified into 3 categories: axial, spinning and "push-pull" modes. For $m = 0$, Eqn. (4) shows that the pressure is identical in every unit cell with no phase difference in the azimuthal direction, i.e. an axial mode. Mode order $m = N/2$ only exists when the number of discrete rotational symmetry is even. In this case, the acoustic field of one burner is in anti-phase with respect to the acoustic field of its two neighbors and, for this reason, is called "push-pull". Spinning modes in the (anti-)clockwise direction appear for Bloch wave numbers of $m = \pm 1, \ldots, \pm(N/2-1)$. Because the system exhibit reflectional symmetry (negligible mean flow in azimuthal direction), these modes are degenerate pairs that share the same eigenfrequency and differ only by their spinning direction.

From the study of one unit cell only, and for all possible values of m, one can assess the response of the complete system accounting for all azimuthal modes [37–39]. The complete system burners-chamber can be reduced to the study of only one unit cell as depicted in Fig. 1. The model is very similar to the one introduced by Parmentier et al. [33], but Bloch theory, by introducing a quasi-periodic boundary condition mutually connecting the left and right boundaries of the unit cell, allows to avoid tedious matrix products to find the dispersion relation.

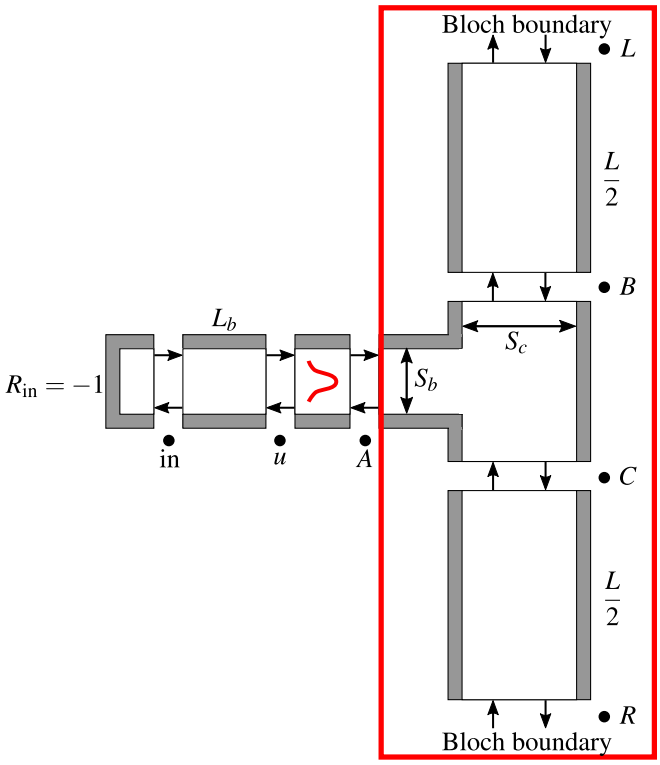

Fig. 1: Network model of one unit cell of an annular chamber exhibiting rotational and reflectional symmetry.

EQUIVALENT LONGITUDINAL BURNER

In order to better understand the underlying physics and further simplify the system, we derive a model and the combustion chamber (red box in Fig. 1) is replaced by its equivalent reflection coefficient. We show that, with Bloch theory, we can reduce a complex annular geometry to an equivalent longitudinal burner.

Modeling of the T-Junction and the Chamber

The T-junction is considered acoustically compact and its volume is null. The chamber does not exhibit any mean flow in the azimuthal direction, therefore, the mass conservation equation integrated over the control volume reduces to conservation of volumetric flow rate:

$$S_c u'_C = S_c u'_B + S_b u'_A \tag{5}$$

The momentum conservation equation applied to an inviscid 1D flow leads to pressure continuity in the junction:

$$p'_C = p'_B = p'_A \tag{6}$$

To investigate ITA modes, it is often more convenient to use Riemann invariants. In this context, we recall the definition of characteristic waves amplitudes

$$f \equiv \frac{1}{2}\left(\frac{p'}{\bar{\rho}c} + u'\right), \quad g \equiv \frac{1}{2}\left(\frac{p'}{\bar{\rho}c} - u'\right) \tag{7}$$

Using Riemann invariants definition from Eqn. (7), Eqn. (5, 6) become

$$\begin{cases} f_C + g_C = f_B + g_B = f_A + g_A & \text{(8a)} \\ f_C - g_C = f_B - g_B + \alpha(f_A - g_A) & \text{(8b)} \end{cases}$$

where $\alpha = S_b/S_c$ is the area ratio between burner and chamber.

The objective is to replace the system T-junction and chamber by the equivalent reflection coefficient seen by the burner, i.e. to express g_A, the wave coming back from the chamber and traveling in the upstream direction as a function of the incoming wave f_A. We define the reflection coefficient $\mathscr{R}_m$ as:

$$g_A = \mathscr{R}_m f_A \tag{9}$$

From the T-junction, plane waves propagate in the chamber to the locations L and R (left and right boundaries of the unit cell respectively, as shown in Fig. 1).

$$\begin{bmatrix} f_R \\ g_R \end{bmatrix} = \begin{bmatrix} e^{-ik\frac{L}{2}} & 0 \\ 0 & e^{ik\frac{L}{2}} \end{bmatrix} \begin{bmatrix} f_C \\ g_C \end{bmatrix}, \quad \begin{bmatrix} f_B \\ g_B \end{bmatrix} = \begin{bmatrix} e^{-ik\frac{L}{2}} & 0 \\ 0 & e^{ik\frac{L}{2}} \end{bmatrix} \begin{bmatrix} f_L \\ g_L \end{bmatrix} \tag{10}$$

Locations L and R are mutually connected with Bloch boundaries as in Haeringer and Polifke [39].

$$\begin{bmatrix} f_R \\ g_R \end{bmatrix} = \begin{bmatrix} e^{i\frac{2\pi m}{N}} & 0 \\ 0 & e^{i\frac{2\pi m}{N}} \end{bmatrix} \begin{bmatrix} f_L \\ g_L \end{bmatrix} \tag{11}$$

Combining Eqn. (9, 10, 11) leads to the homogeneous linear system of equations defined through the matrix

$$\underbrace{\begin{bmatrix} 1-e^{i\left(\frac{2\pi m}{N}+kL\right)} & 1-e^{i\left(\frac{2\pi m}{N}-kL\right)} \\ e^{i\left(\frac{2\pi m}{N}+kL\right)} - \alpha\frac{1-\mathscr{R}_m}{1+\mathscr{R}_m} - 1 & 1-e^{i\left(\frac{2\pi m}{N}-kL\right)} - \alpha\frac{1-\mathscr{R}_m}{1+\mathscr{R}_m} \end{bmatrix}}_{\mathbf{M}(\omega,m)} \tag{12}$$

The linear system of equations for f_B and g_B reads

$$\mathbf{M}(\omega,m) \begin{bmatrix} f_B \\ g_B \end{bmatrix} = \begin{bmatrix} 0 \\ 0 \end{bmatrix} \tag{13}$$

The detailed derivation can be found in Appendix A. The system shows non trivial solution if the determinant of $\mathbf{M}(\omega,m)$ is null, which gives a condition for the reflection coefficient:

$$\mathscr{R}_m(\omega) = \frac{-2\cos\left(\frac{2\pi m}{N}\right) + 2\cos(\mathrm{He}) - i\alpha\sin(\mathrm{He})}{2\cos\left(\frac{2\pi m}{N}\right) - 2\cos(\mathrm{He}) - i\alpha\sin(\mathrm{He})} \tag{14}$$

with the Helmholtz number being defined as $\mathrm{He} = \dfrac{\omega L}{c}$. Note that $\mathscr{R}_m(\omega)$ depends on the frequency and the mode order.

Interpretation of the Reflection Coefficient

The equivalent reflection coefficient $\mathscr{R}_m(\omega)$ depends not only on the frequency ω, as it is often the case for a boundary conditions, but also on the azimuthal mode order m. Depending on the order of the mode present in the

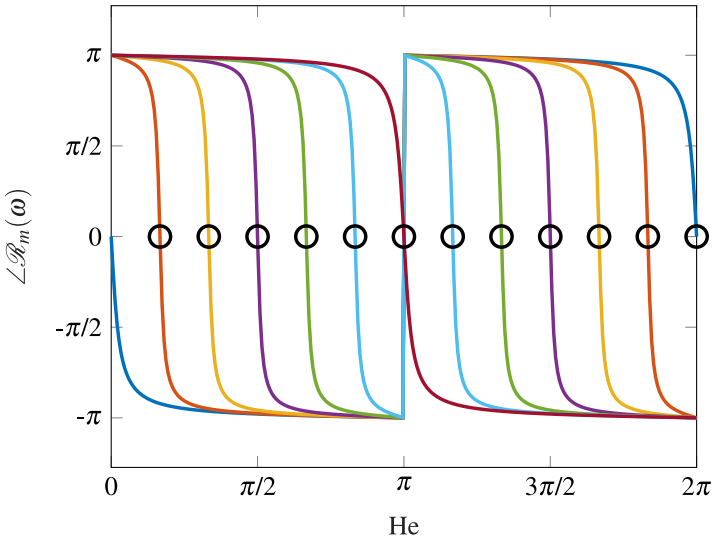

Fig. 2: Phase of the equivalent reflection coefficient $\mathscr{R}_m$ for an annular combustor with 12 burners for the azimuthal modes $m = 0$ —, $m = 1$ —, $m = 2$ —, $m = 3$ —, $m = 4$ —, $m = 5$ —, $m = 6$ —. Circles: passive acoustic modes of the combustion chamber.

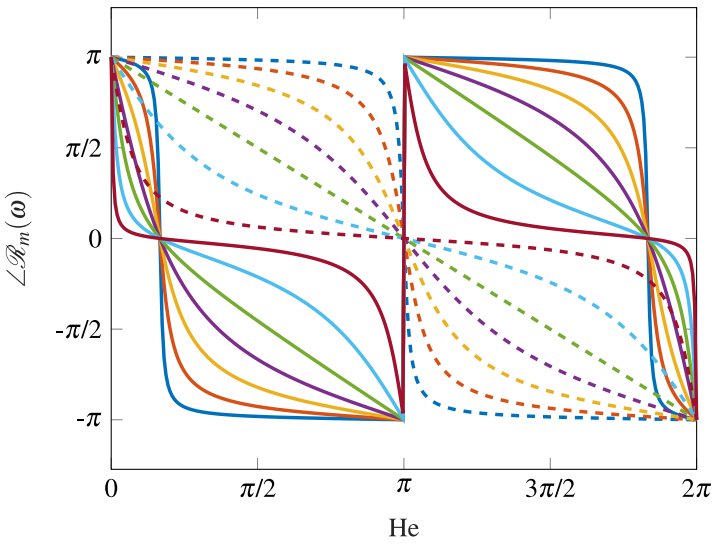

Fig. 3: Phase of the equivalent reflection coefficient for an annular combustor with 12 burners with area ratio between burner and chamber $\alpha = S_b/S_c = 1/20$ —, $\alpha = 1/5$ —, $\alpha = 1/2$ —, $\alpha = 1$ —, $\alpha = 2$ —, $\alpha = 5$ —, $\alpha = 20$ —. Full lines: azimuthal mode $m = 1$. Dashed lines: azimuthal mode $m = 6$.

chamber, the burner tube is exposed to a different outlet acoustic boundary condition.

At zero growth rate, Eqn. (14) shows that the gain of the reflection coefficient is trivially unity at all frequencies and for all mode orders. This result was to be expected because no loss mechanism was taken into account and no energy is added to the system. On the other hand, the phase is different for all the modes and changes with the frequency. Figure 2 presents the evolution of the phase as a function of the dimensionless frequency He for an annular

combustor of 12 burners and with an area ratio of $\alpha = 1/15$. We observe that, in the zero frequency limit, the chamber behaves as a hard wall ($\mathscr{R}_0 = 1$) for the axial mode whereas it behaves as an open end ($\mathscr{R}_m = -1$) for all other azimuthal mode orders. Corresponding observations for a can-annular combustor were made by Ghirardo et al. [38] and were explained mathematically by the fact that the Galerkin series of an axial mode has a Helmholtz mode at frequency $\omega = 0$. We can also interpret it physically. The mode is of axial type, the acoustic field is uniform in the azimuthal direction, the T-junction is compact, so the boundary condition seen by the burner is exactly the same as the one at the inlet of the turbine ($R_{\text{out}} = 1$ in this case), thus explaining the phase going to 0 in the low frequency limit.

For the other modes, the phase is rather close to either π or $-\pi$ but changes abruptly from one to the other with a periodic pattern. Indeed, for each mode, at a given frequency, the reflection coefficient becomes $\mathscr{R}_m = 1$. From Eqn. (14), we can show analytically that:

$$\begin{aligned} \mathscr{R}_m(\omega) = 1 &\iff \cos(\mathrm{He}) = \cos\left(\frac{2\pi m}{N}\right) \\ &\iff \mathrm{He} = kL = 2\pi h \pm \frac{2\pi m}{N}, \quad h \in \mathbb{N} \\ &\iff \frac{kP_c}{2} = (Nh \pm m)\,\pi, \quad h \in \mathbb{N} \end{aligned} \tag{15}$$

where $P_c = NL$ is the total perimeter of the chamber. $\mathscr{R}_m = 1$ is the special case where the burner tube has a velocity node at its outlet and therefore the flame is not influencing at all the chamber. In that sense, the burner tube is decoupled, and the chamber is a simple annular duct whose eigenfrequency (or resonance frequency) is defined by Eqn. (15). These frequencies correspond to the passive acoustic modes of the chamber. For a pure chamber mode, the burner outlet is equivalent to a hard wall.

The area jump between burners and chamber will also strongly influence the equivalent reflection coefficient. Figure 3 show the evolution of the phase for the modes $m = 1$ and $m = N/2$ with α varying from 0.05 to 20. When α is large, the phase tends to be 0 for all frequencies, which means $\mathscr{R}_m = 1$. This is the limit case of a can-annular configuration: the burner tube is similar to a can exposed to a choked exit. In contrast, when α is small, $\mathscr{R}_m$ tends to be equal to -1, the burner tube ends in a large vessel (combustion chamber), which is a representation of an annular configuration. Ghirardo et al. [38] introduced the notion of equivalent reflection coefficient for a 2D can-annular configuration. In the present study, we derived a general 1D expression for the equivalent reflection coefficient seen by a duct terminating in an annular chamber. Although in this paper an annular combustor is considered, the model could easily be applied to a can-annular configuration. This 1D model is simple but gives good qualitative agreement

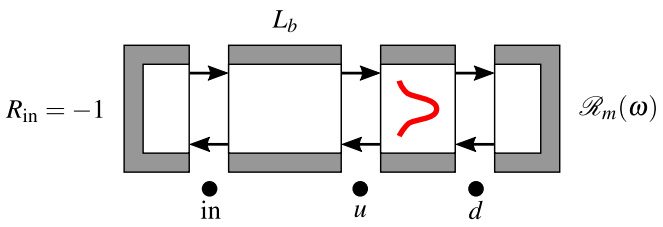

Fig. 4: Annular geometry reduced to a single longitudinal burner. The outlet reflection coefficient $\mathscr{R}_m(\omega)$ depends on frequency and mode order and models the behavior of the combustion chamber.

compared to 2D and 3D computations [38, 48]. Note that the derivation also holds for the plenum side; the impact of the plenum could be investigated in future work with the same model.

Reduction of the System to a Longitudinal Burner

In the previous section, we showed that the entire chamber can be modeled with an equivalent reflection coefficient $\mathscr{R}_m(\omega)$ that depends on frequency ω and azimuthal order m. The unit cell considered in Fig. 1 can therefore be further reduced into $N/2$ simpler sub-systems which consists only of longitudinal burners as depicted in Fig. 4. It is remarkable that a complex annular system can be analytically reduced to such a simple longitudinal configuration. Such burners have been already studied in the context of ITA modes.

Following the approach proposed by Silva et al. [10], the equations for such a configuration are written as:

$$\begin{bmatrix} -1 & R_{\text{in}} & 0 & 0 \\ T_{11} & T_{12} & -1 & 0 \\ T_{21} & T_{22} & 0 & -1 \\ 0 & 0 & \mathscr{R}_m(\omega) & -1 \end{bmatrix} \begin{bmatrix} f_{\text{in}} \\ g_{\text{in}} \\ f_d \\ g_d \end{bmatrix} = \begin{bmatrix} 0 \\ 0 \\ 0 \\ 0 \end{bmatrix} \tag{16}$$

where T_{ij} are the coefficients of the overall acoustic transfer matrix formed by the propagation of the waves inside the burners tubes and the flame.

$$T = \frac{1}{2} \begin{bmatrix} \xi + 1 + \theta \mathscr{F}(\omega) & \xi - 1 - \theta \mathscr{F}(\omega) \\ \xi - 1 - \theta \mathscr{F}(\omega) & \xi + 1 + \theta \mathscr{F}(\omega) \end{bmatrix} \begin{bmatrix} e^{-i\omega L_b/c_c} & 0 \\ 0 & e^{i\omega L_b/c_c} \end{bmatrix} \tag{17}$$

Table 1: Numerical parameters of the lab-scale combustor

Geometrical parameters	
N [-]	12
α [-]	1/15
L_b [m]	1.5×10^{-2}
L [m]	5×10^{-2}

Thermodynamics parameters	
c_u [m s^{-1}]	341
T_d/T_u [-]	4
n [-]	1
τ [s]	2×10^{-3}

The determinant of the system matrix from Eqn. (16) leads to the corresponding dispersion relation

$$T_{22} - \mathscr{R}_m(\omega)T_{12} - T_{21} + \mathscr{R}_m(\omega)T_{11} = 0 \tag{18}$$

Equation (18) is highly non-linear and can generally not be solved analytically. To overcome the problem, the system is computed with taX. taX is an open-source Matlab package developed by the TFD group to build and solve low-order thermoacoustic network models [49, 50]. With the use of finite differences in a state-space framework, taX reduces Eqn. (18) to a generalized linear eigenvalue problem, which facilitates the use of direct solvers to compute the complete spectrum of eigenvalues and eigenmodes. This key feature proves to be crucial to find ITA modes in a simple manner. Mensah [51] and Buschmann et al. [23] have shown that if, instead, the non-linear eigenvalue problem is solved by iterative methods, finding ITA modes remains difficult as they are associated with small basin of attraction.

ON THE ORIGIN OF ITA CLUSTERS

In this section, we apply our model to a lab-scale combustor, which has chamber cavity modes far away from the pure ITA fundamental frequency, and explain the origin of ITA clusters. We also explain why the damping of ITA modes increases with the azimuthal order.

Equivalent Rijke Tube

We apply our model to a realistic lab-scale combustor. Geometrical and thermodynamics parameters are given in Tab. 1. The time delay of the flame model is $\tau = 2\,\text{ms}$, so the pure ITA fundamental frequency is evaluated at $f_{\text{ITA}} = 250\,\text{Hz}$. The length between 2 burners L is rather small, the total length of the chamber is 0.6 m, which guarantees chamber cavity modes at much higher frequencies than the pure ITA frequency. Indeed the first azimuthal passive chamber mode is evaluated at $f = c_d/P_c = 1090\,\text{Hz}$. The combustor has 12 burners therefore ITA modes up to

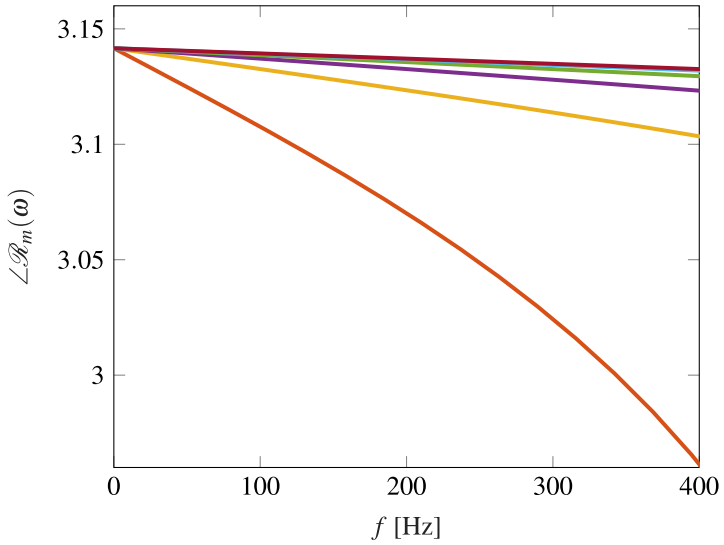

Fig. 5: Phase of the equivalent reflection coefficient $\mathscr{R}_m$ in the case where the chamber mode is far away from the ITA mode. Colors indicate the azimuthal order as defined in Fig. 2.

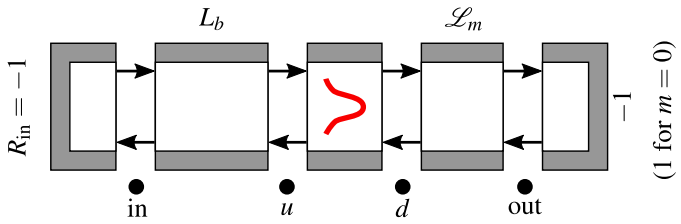

Fig. 6: Equivalent Rijke tube with fully reflecting boundary conditions. The equivalent length $\mathscr{L}_m$ varies with the azimuthal order and models the behavior of the chamber.

order 6 will arise.

Figure 5 presents the equivalent reflection coefficient in the frequency range of interest [0–400 Hz]. In Fig. 2, it corresponds to a Helmholtz number He between 0 and 0.25. In that frequency range, for mode order m between 1 and $N/2$, starting from π at zero frequency, the phase of each mode depends linearly on the frequency He. Therefore, for each m, the phase is modeled by the simple equation $\angle \mathscr{R}_m = \pi - a_m \text{He}$, where the slope of the line is the positive coefficient a_m. Because the gain of $\mathscr{R}_m$ is unity, the equivalent reflection coefficient writes:

$$\mathscr{R}_m(\omega) = -e^{-ia_m \text{He}} = -e^{-i2k\mathscr{L}_m}, \quad \mathscr{L}_m = \frac{a_m L}{2c_d} \tag{19}$$

From Eqn. (19), we can directly see that the reflection coefficient $\mathscr{R}_m$ is equivalent to a duct of length $\mathscr{L}_m$ terminated by an open end. Therefore, the longitudinal burner introduced in Fig. 4 can be transformed into the completely

equivalent, yet simpler, Rijke tube depicted in Fig. 6. The boundary conditions are fully reflecting and are independent of the frequency. The length of the equivalent duct $\mathscr{L}_m$ varies with the mode order m: the lower the azimuthal order, the longer the equivalent duct (the line is steeper for low azimuthal order in Fig. 5). Following the exact same reasoning for the axial mode, the system can also be reduced to a Rijke tube but with a closed end as outlet boundary condition. Indeed, in Fig. 2, we can see that the phase of the axial mode is zero in the low frequency limit.

Thermoacoustic modes of acoustic or ITA origin have already been studied for the Rijke configuration. Hosseini et al. [19] showed that, for fully reflecting boundary conditions, when the pure ITA mode is far away from the passive acoustic modes, the two do not interplay and the frequency associated with the thermoacoustic mode of ITA origin stays close to the pure ITA frequency. The same result can also be observed in the star shape introduced by Silva et al. [21] or in other recent studies by Orchini et al. [22] and Mukherjee and Shrira [15]. For a pure ITA frequency away enough from the passive acoustic mode, the trajectory in the complex plane of the thermoacoustic mode of ITA origin will be a straight line when varying n (Fig.6 from [22]): the growth rate of the mode is changing with the interaction index but the frequency remains approximately constant.

The annular geometry has been reduced to a simple Rijke tube configuration. For this reduced system, we need to compare the pure ITA frequency $f_{\mathrm{ITA}} = \frac{1}{2\tau}$ to the passive acoustic mode of the Rijke tube of total length $L_{\mathrm{tot}} = L_b + \mathscr{L}_m$. For lab-scale combustors, the burners are rather short, of the order of magnitude of a centimeter (1.5 cm in our application case). Following Eqn. (19), because the speed of sound is usually high in the chamber, it is straight forward to prove analytically that, for all azimuthal order m, $\mathscr{L}_m$ is always at least one order of magnitude lower than L, the distance between two burners. For such combustors, the effective length $\mathscr{L}_m$ is small, of the order of magnitude of a centimeter for low azimuthal mode order, and much smaller for higher mode order. Therefore, the total length of the equivalent Rijke tube is of the order of magnitude of 1–10 cm, which leads to passive acoustic modes at high frequencies (above 1000 Hz). On the other hand, because the time delay of the flame response is usually between 1–2 ms, the pure ITA fundamental frequency $f_{\mathrm{ITA}} = \frac{1}{2\tau}$ will be below 500 Hz. The passive acoustic mode is far away from the pure ITA fundamental frequency. Therefore, for all azimuthal mode order m, thermoacoustic modes of acoustic and ITA origin do not interplay: ITA modes of various azimuthal order will remain close to the pure ITA frequency, and thus creating clusters of ITA modes. Note that this result may not directly apply for industrial configurations where the dimensions are much more significant and could lead to ITA-acoustic interplay. Similarly, this hypothesis is also not valid for clusters of ITA harmonics which are located at higher frequencies. In both cases, clusters are still present but may not contain all azimuthal mode order: some modes may shift and be offset from their respective clusters. This will be develop in a following section.

Figure 7 presents the spectrum of our application case. The equivalent Rijke tube reduced model (squares) shows

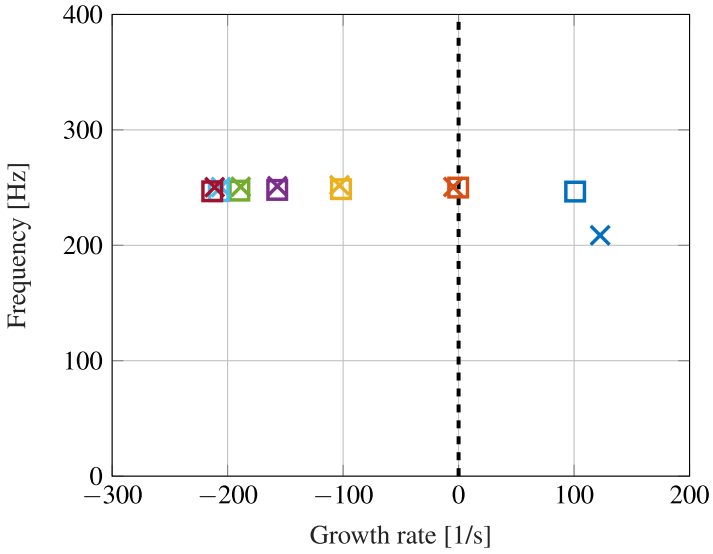

Fig. 7: Thermoacoustic spectrum where ITA modes show various azimuthal order. Crosses: full system. Squares: equivalent Rijke tube model. Colors indicate the azimuthal order as defined in Fig. 2.

excellent agreement with the full system predictions (crosses) computed by taX. Some discrepancy is observed for the axial mode, that is explained in a next section. Thermoacoustic modes of acoustic origin are completely out of the frequency range of interest and do not interplay with thermoacoustic modes of ITA origin. The latter, as expected, lie around the pure ITA frequency, at 250 Hz. Their growth rate changes with the mode order: modes with higher azimuthal order are more damped, as it was also observed by Buschmann et al. [23, 24]. We explain this phenomena in the next section.

On the Damping of ITA Modes

In this section, we want to investigate how the damping of an ITA mode is affected by the azimuthal order. As a first case, we consider a Rijke tube, as depicted in Fig. 6, where the effective length $\mathscr{L}_m$ is about the same length as the burner L_b. The flame is located approximately in the middle of the Rijke tube, away from the boundaries. This first case models a low azimuthal order ITA mode. This one dimensional thermoacoustic system is studied here by means of a phasor analysis. The spatial evolution of Riemann invariants f and g along the system is modeled with phasors rotating in the complex plane. Such analysis was previously applied in the context of ITA modes [17, 18] and has proven to be convenient to study linear stability.

For simplicity, we consider a mode at the stability limit (zero growth rate) in order to impose a fixed length to each phasor. A phasor diagram associated with the acoustic waves f and g is displayed in Fig. 8. For convenience, it is assumed that the phasor f_{in} is aligned with the real axis of the complex plane. The reflecting condition at the inlet

implies that $g_{in} = -f_{in}$. The acoustic wave f will travel from the inlet to the flame along the duct of length L_b. The wave at the location u, upstream of the flame, is related to the inlet by $f_u = f_{in}e^{-i\omega L_b/c_u}$. On the phasors plot, this leads to a rotation of an angle $\varphi_u = \omega L_b/c_u$. Conversely, the g phasor will rotate with the same angle φ_u but in the opposite direction. Sum and subtraction of the phasors yields the acoustic phasors p' and u' respectively.

The same analysis is performed from the downstream boundary. The top of Fig. 9 presents the phasors plot rotating from the outlet to the location just downstream the flame. For the sake of simplicity in the diagrams, we assume $\bar{\rho}_u c_u = \bar{\rho}_d c_d = 1$. Such a simplification allows to define $p' = f + g$ and $u' = f - g$. Note that taking into account the temperature jump across the flame would lead to the same conclusion. The direction of f_{out} and g_{out} are known because the outlet boundary condition needs to be satisfied, but their length is not known a priori. From the outlet, f and g rotate by an angle $\varphi_d = \omega \mathscr{L}_m/c_d$. Note that their sense of rotation is opposed with respect to the ones of f_u and g_u because waves propagate now from the downstream side. The direction of the phasors f_d and g_d downstream the flame is therefore known. Jump conditions across the flame need to be fulfilled. Knowing the direction and the magnitude of p'_u, and knowing the directions of f_d and g_d, it is possible to geometrically construct the lengths of the latter. Using Eqn. (7, 2), determining the heat release $\dot{q}'$ is straight forward.

We now consider a second case where the upstream part of the flame is identical, but the effective length $\mathscr{L}_m$ downstream the flame is shorter, about half of the length of the first case. The flame is now located closer to the outlet boundary. This second case is representative of a higher azimuthal order ITA mode. Because the upstream part is unchanged, the upstream phasor plot is identical to Fig. 8. On the other hand, the downstream phasor plot differs. Because $\mathscr{L}_m$ is smaller, the phasors will rotate from the outlet with a smaller angle φ_d, as shown in the bottom of Fig. 9. Because the pressure continuity at the flame still needs to be fulfilled, the length of f_d and g_d should be adapted accordingly. As a result, the phasors f_d and g_d are longer than in the first case, which leads to a longer phasor of velocity u'_d. The latter implies that Eqn. (2) is satisfied for larger values of $\dot{q}'$

Summarizing, we have shown that $\dot{q}'$ for the second case is larger than $\dot{q}'$ for the first case in the region of marginal stability. Accordingly, we conclude that the second system requires more energy than the first one to remain neutrally stable, and, therefore, its critical interaction index n_c is higher. Said differently, if we inject the same amount of energy $\dot{q}'$ in both systems (i.e. if both systems have the same interaction index n), the second one will exhibit higher damping. The proposed phasor analysis sheds a light on the spectrum shown in Fig. 7: the effective length $\mathscr{L}_m$ decreases with the mode order m, therefore higher azimuthal order ITA modes are more damped.

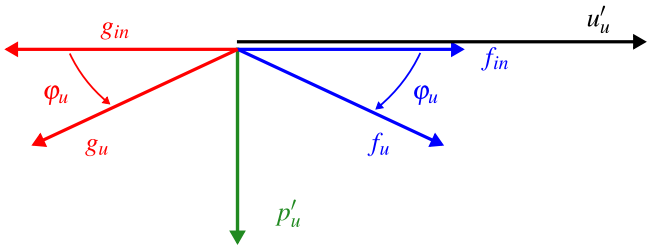

Fig. 8: Phasors diagram of acoustic waves f and g at the inlet and at the location u, just upstream of the flame. Sum and subtraction of these phasors yields the acoustic phasors p' and u'.

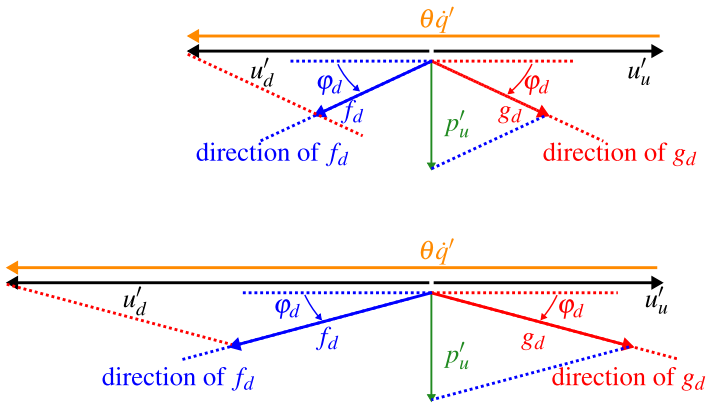

Fig. 9: Phasors diagram of acoustic waves f and g at the outlet and at the location d, just downstream of the flame. Top: ITA mode with a low azimuthal order. Bottom: ITA mode with a higher azimuthal order.

ITA MODES DRIFTING AWAY FROM THEIR CLUSTER

In Fig. 7, we observed that the axial mode is slightly offset from the cluster: its frequency is around 222.7 Hz, compared to the 250 Hz of the pure ITA frequency. The reduced Rijke tube model is not able to capture this drift. In this section, we investigate the cause of ITA modes shifting away from their cluster. We will demonstrate that this phenomena takes place when the π-criterion [8] is broken. Two causes are identified.

The first cause is the gain or losses introduced by acoustic boundaries. The gain of the equivalent reflection coefficient as defined in Eqn. (14) is not always unity for complex-valued frequencies. Figure 10 shows the evolution of the gain of $\mathscr{R}_0$ with respect to frequency and growth rate around the pure ITA frequency. The gain drifts from unity by up to 20%. Hence, away from zero growth rate, the boundary is not anymore fully reflecting but introduces some losses/amplification. For azimuthal order, as shown in Fig. 11 for $m = 1$, the gain of $\mathscr{R}_m$ is unity and uniform away from the passive acoustic chamber mode $f = \frac{mc_d}{P_c}$. But, in the region close to the passive chamber mode, at non zero growth rate, the gain of $\mathscr{R}_m$ exhibits important variations, also transforming the fully reflecting boundaries into boundaries with losses/gain.

The second cause is the range of validity of the model where the phase $\mathscr{R}_m$ is considered linear with respect to

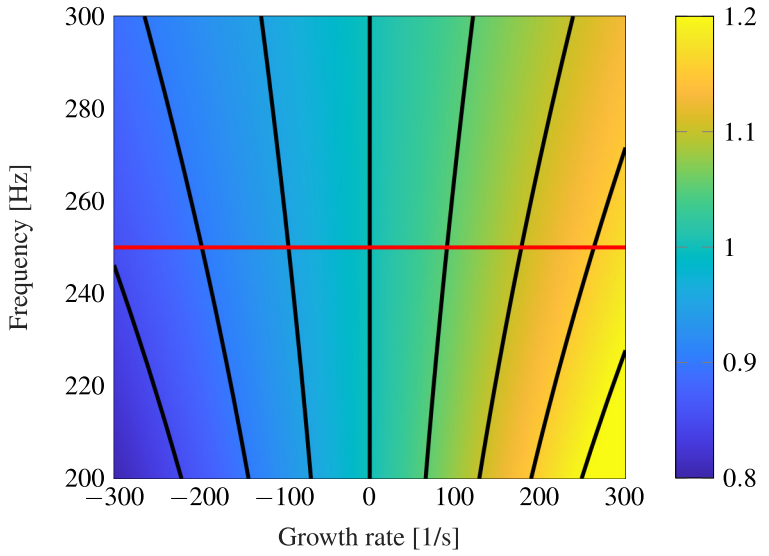

Fig. 10: Gain of the equivalent reflection coefficient $\mathscr{R}_0$ as a function of frequency and growth rate. Red line: pure ITA frequency. Black lines: isolines varying from 0.85 to 1.2 with an increment of 0.05. Away from the real axis, the gain differs from unity; the boundary is not fully reflecting but introduces damping/amplification.

frequency. Indeed, this model is valid for low frequencies and up to a certain extent. For higher frequencies, the phase of the equivalent reflection coefficient $\mathscr{R}_m$ stops evolving linearly with He, and is rather similar to Fig. 2. The approximation of the system by a Rijke tube is not valid anymore. Nevertheless, the system can still be modeled by a longitudinal combustor with an outlet boundary that depends on the frequency as in Fig. 4.

The two aforementioned effects lead to ITA modes drifting away from their pure ITA frequency. When the boundaries are fully reflecting, p' and u'_d are orthogonal, as illustrated on the left side of Figure 12. The velocities u'_u and u'_d are aligned with the real axis but have opposite directions. The phase difference between u'_u and u'_d is $\varphi = \pi$. It is possible to estimate the frequency of the ITA mode $f = \frac{\varphi}{2\pi\tau} = \frac{1}{2\tau}$. We here retrieve the classic π-criterion to identify ITA modes [8]. However, when the outlet boundary is not fully reflecting, p' and u'_d are not orthogonal. The phase between the velocities u'_u and u'_d changes and therefore, the π-criterion is broken, as depicted on the right side of Fig. 12. The ITA mode has frequency different from the pure ITA frequency, i.e. the mode is offset from its cluster.

It is interesting to notice from Fig. 2 that the phase of $\mathscr{R}_m$ is linearly dependent on frequency over a wider frequency range for modes with a higher azimuthal order. The higher the mode order, the larger the region of validity of the Rijke tube model with fully reflecting boundaries. This means that, for ITA harmonics, modes with low azimuthal order are the first to deviate from the cluster. Figure 13 presents the spectrum of an annular chamber with ITA fundamental modes and first harmonics. Note that, because the full system can be reduced to a longitudinal burner, the analytical expression of the frequency spacing between ITA modes $\Delta f = 1/\tau$ derived by Emmert et al. [7] applies here. Therefore, this explains the constant frequency spacing between clusters. In the first cluster, all the modes are

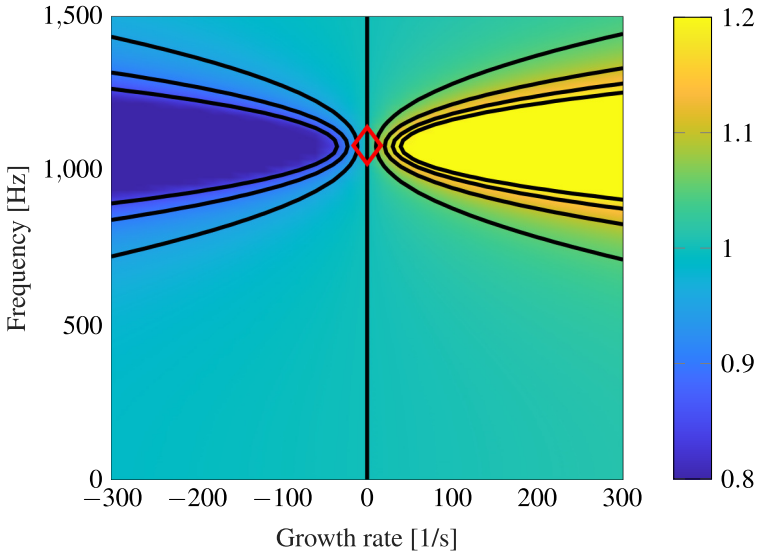

Fig. 11: Gain of the equivalent reflection coefficient $\mathscr{R}_1$ as a function of frequency and growth rate. Diamond: passive acoustic mode of the chamber. Black lines: isolines varying from 0.85 to 1.2 with an increment of 0.05. In the region of the passive acoustic chamber mode, the gain differs from unity; the boundary is not fully reflecting but introduces damping/amplification. Results are similar for other mode orders. Note that the frequency range of interest is different from Fig. 10.

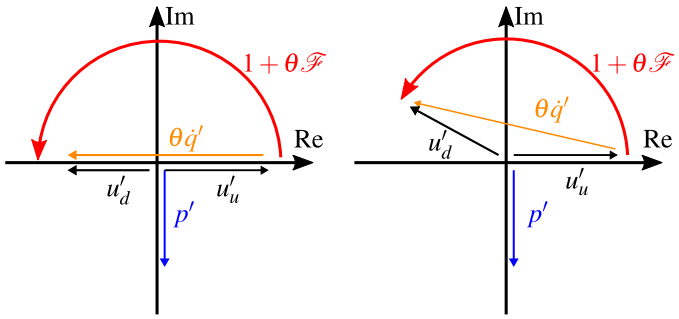

Fig. 12: Phasors diagram in the case of fully reflecting boundary conditions (left) and non fully reflecting boundary conditions (right). For the second case, the π-criterion for ITA modes is not fulfilled. The mode will shift away from the pure ITA frequency.

around the pure ITA frequency, besides the axial mode, as explained earlier. In the second cluster, the first azimuthal mode is also offset from its cluster. Indeed, at such frequency, the Rijke tube approximation is not valid, the outlet boundary of the equivalent longitudinal burner is not fully reflecting and the π-criterion is not fulfilled: the ITA mode cannot be around the pure ITA frequency of the first harmonic. The same observations can be made by considering higher harmonics: the second azimuthal order mode will deviate, then the third and so on.

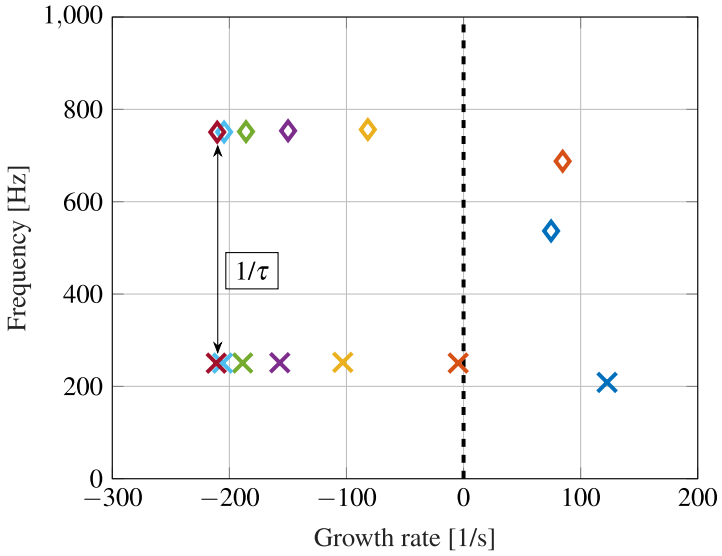

Fig. 13: Thermoacoustic spectrum of an annular chamber. In the first cluster, only the axial mode is offset. In the second one, both axial and first azimuthal order are offset from their cluster. Crosses: first ITA cluster. Diamonds: second ITA cluster. Colors indicate the azimuthal order as defined in Fig. 2.

CONCLUSION

In this paper we proposed a new approach that combines network models and Bloch theory to describe ITA modes in an annular chamber. Bloch boundary conditions are convenient to use because they enable us to limit the study to a single unit cell and reconstruct the results for the full system without loss of accuracy. We analytically derived a reflection coefficient that models the chamber and how the latter affects the acoustic in the burner. With the use of Bloch theory and Riemann invariants, an annular configuration, where axial and radial dimensions are negligible compared to the azimuthal direction, can be reduced to a simple equivalent longitudinal combustor. The equivalent reflection coefficient depends on the frequency and the azimuthal order of the mode present in the chamber. The area ratio between burners and chamber also widely influences the coupling between the latter and consequently the acoustic response of the burners. The model was derived without loss of generality and is suitable to describe various cases, from annular geometries to can-annular configurations where the burners dimensions are much more significant and the chamber consists only of a small cross-talk area.

The suggested model was applied to a lab-scale combustor. For such configurations, when the acoustic mode of the chamber is far away from the pure ITA frequency, we showed that the longitudinal burner can be reduced to an even simpler model, a Rijke tube with fully reflecting boundaries. The length of the Rijke tube and the flame position in it depends on the azimuthal mode considered. But, because the acoustic mode of the Rijke tube and the ITA frequency are away from each other, thermoacoustic modes of acoustic and ITA origin do not interplay with each

other. Therefore, for every azimuthal order, each ITA mode has a frequency close to the pure ITA frequency: this explains the origin of ITA clusters.

The reduced Rijke tube model also allowed us to explain the structure of the spectrum. The flame position in the Rijke tube varies with the azimuthal order, the higher the order, the closer the flame is to the outlet boundary. With the use of a phasors analysis for ITA modes, we showed that, for a flame close to the outlet, the system requires more energy to stay at the stability limit than for a case where the flame is far from the outlet. Said differently, for a given heat release rate, the closer the flame to the outlet, the more damped the mode. This result explains the spectrum structure where ITA modes of higher order are always more damped.

Finally, we investigated the phenomenon of ITA modes drifting away from their clusters. When the outlet boundary is not fully reflecting, pressure and velocity are not orthogonal and the π-criterion is broken. The frequency of the ITA mode is different from its pure ITA frequency, i.e. the mode is offset from its cluster. We demonstrated that low azimuthal order modes deviates first. The impact of the plenum and a possible interplay between thermoacoustic modes of ITA and acoustic origin can be investigated in future work.

ACKNOWLEDGEMENTS

This project has received funding from the European Union's Horizon 2020 research and innovation programme under Grant Agreement No 765998 *Annular Instabilities and Transient Phenomena in Gas Turbine Combustors* (ANNULIGhT). The authors gratefully acknowledge the Research Association for Combustion Engines (Forschungsvereinigung Verbrennungskraftmaschinen e.V. FVV, project number 6012700) for the financial support to Matthias Haeringer. The authors would also like to thank Max Meindl and Felix Schily for valuable discussions.

REFERENCES

[1] Lieuwen, T., and McManus, K., 2003. "Introduction: Combustion Dynamics in Lean-Premixed Prevaporized (LPP) Gas Turbines". *Journal of Propulsion and Power,* ***19***(5), pp. 721–721.

[2] Poinsot, T., 2017. "Prediction and Control of Combustion Instabilities in Real Engines". *Proceedings of the Combustion Institute,* ***36***, pp. 1–28.

[3] Lieuwen, T., and Yang, V., eds., 2005. *Combustion Instabilities in Gas Turbine Engines: Operational Experience, Fundamental Mechanisms, and Modeling*, Vol. 210 of *Progress in Astronautics and Aeronautics*. AIAA.

[4] Bomberg, S., Emmert, T., and Polifke, W., 2015. "Thermal Versus Acoustic Response of Velocity Sensitive Premixed Flames". *Proceedings of the Combustion Institute,* ***35***(3), pp. 3185–3192.

[5] Gentemann, A., and Polifke, W., 2007. "Scattering and generation of acoustic energy by a premix swirl burner". In Volume 2: Turbo Expo 2007, GT2007-27238, ASMEDC, pp. 125–133.

[6] Polifke, W., 2011. "Thermo-Acoustic Instability Potentiality of a Premix Burner". In European Combustion Meeting, ECM2011, British Section of the Combustion Institute.

[7] Emmert, T., Bomberg, S., and Polifke, W., 2015. "Intrinsic Thermoacoustic Instability of Premixed Flames". *Combustion and Flame,* ***162***(1), pp. 75–85.

[8] Hoeijmakers, M., Lopez Arteaga, I., Kornilov, V., Nijmeijer, H., and de Goey, P., 2013. "Experimental Investigation of Intrinsic Flame Stability". In European Combustion Meeting, ECM2013, Scandinavian-Nordic Section of the Combustion Institute.

[9] Hoeijmakers, M., Kornilov, V., Lopez Arteaga, I., de Goey, P., and Nijmeijer, H., 2014. "Intrinsic Instability of Flame-Acoustic Coupling". *Combustion and Flame,* ***161***(11), Nov., pp. 2860–2867.

[10] Silva, C. F., Emmert, T., Jaensch, S., and Polifke, W., 2015. "Numerical Study on Intrinsic Thermoacoustic Instability of a Laminar Premixed Flame". *Combustion and Flame,* ***162***(9), pp. 3370–3378.

[11] Courtine, E., Selle, L., and Poinsot, T., 2015. "DNS of Intrinsic Thermoacoustic Modes in Laminar Premixed Flames". *Combustion and Flame,* ***162***(11), pp. 4331–4341.

[12] Emmert, T., Bomberg, S., Jaensch, S., and Polifke, W., 2017. "Acoustic and Intrinsic Thermoacoustic Modes of a Premixed Combustor". *Proceedings of the Combustion Institute,* ***36***(3), pp. 3835–3842.

[13] Lieuwen, T. C., 2012. *Unsteady Combustor Physics*. Cambridge University Press, New York, N.Y., USA.

[14] Dowling, A. P., and Stow, S. R., 2003. "Acoustic Analysis of Gas Turbine Combustors". *Journal of Propulsion and Power,* ***19***(5), pp. 751–764.

[15] Mukherjee, N., and Shrira, V., 2017. "Intrinsic Flame Instabilities in Combustors: Analytic Description of a 1-D Resonator Model". *Combustion and Flame,* ***185***, pp. 188–209.

[16] Eckstein, J., and Sattelmayer, T., 2006. "Low-order modeling of low-frequency combustion instabilities in aeroengines". *Journal of Propulsion and Power,* ***22***(2), pp. 425–432.

[17] Ghani, A., Steinbacher, T., Albayrak, A., and Polifke, W., 2019. "Intrinsic thermoacoustic feedback loop in turbulent spray flames". *Combustion and Flame,* ***205***(7), pp. 22–32.

[18] Albayrak, A., Steinbacher, T., Komarek, T., and Polifke, W., 2017. "Convective Scaling of Intrinsic Thermo-Acoustic Eigenfrequencies of a Premixed Swirl Combustor". *Journal of Engineering for Gas Turbines and Power,* ***140***(4), Nov., p. 041510.

[19] Hosseini, N., Kornilov, V., Lopez Arteaga, I., Polifke, W., Teerling, O., and de Goey, L., 2018. "Intrinsic thermoacoustic modes and their interplay with acoustic modes in a Rijke burner". *International Journal of Spray*

and Combustion Dynamics, ***10***(4), Dec., pp. 315–325.

[20] Sogaro, F. M., Schmid, P. J., and Morgans, A. S., 2019. "Thermoacoustic interplay between intrinsic thermoacoustic and acoustic modes: Non-normality and high sensitivities". *Journal of Fluid Mechanics,* ***878***, pp. 190–220.

[21] Silva, C., Yong, K. J., and Magri, L., 2019. "Thermoacoustic Modes of Quasi-One-Dimensional Combustors in the Region of Marginal Stability". *Journal of Engineering for Gas Turbines and Power,* ***141***(2), Feb., p. 021022.

[22] Orchini, A., Silva, C. F., Mensah, G. A., and Moeck, J. P., 2020. "Thermoacoustic modes of intrinsic and acoustic origin and their interplay with exceptional points". *Combustion and Flame,* ***211***, pp. 83–95.

[23] Buschmann, P. E., Mensah, G. A., Nicoud, F., and Moeck, J. P., 2019. "Solution of Thermoacoustic Eigenvalue Problems with a Non-Iterative Method". In ASME Turbo Expo 2019: Turbomachinery Technical Conference & Exposition, GT2019-90834, ASME.

[24] Buschmann, P. E., Mensah, G. A., and Moeck, J. P., 2020. "Intrinsic thermoacoustic modes in an annular combustion chamber". *Combustion and Flame,* ***214***, Apr., pp. 251–262.

[25] Staffelbach, G., Gicquel, L. Y. M., Boudier, G., and Poinsot, T., 2009. "Large Eddy Simulation of self excited azimuthal modes in annular combustors". *Proceedings of the Combustion Institute,* ***32***(2), pp. 2909–2916.

[26] Wolf, P., Staffelbach, G., Gicquel, L. Y. M., Müller, J.-D., and Poinsot, T., 2012. "Acoustic and Large Eddy Simulation studies of azimuthal modes in annular combustion chambers". *Combustion and Flame,* ***159***(11), Nov., pp. 3398–3413.

[27] Avdonin, A., Meindl, M., and Polifke, W., 2019. "Thermoacoustic analysis of a laminar premixed flame using a linearized reacting flow solver". *Proceedings of the Combustion Institute,* ***37***, pp. 5307–5314.

[28] Gikadi, J., 2013. "Prediction of Acoustic Modes in Combustors using Linearized Navier-Stokes Equations in Frequency Space". PhD Thesis, Technische Universität München, Garching, Germany, Nov.

[29] Schulze, M., Hummel, T., Klarmann, N., Berger, F. M., Schuermans, B., and Sattelmayer, T., 2017. "Linearized Euler Equations for the Prediction of Linear High-Frequency Stability in Gas Turbine Combustors". *Journal of Engineering for Gas Turbines and Power,* ***139***(3), Mar., p. 031510.

[30] Nicoud, F., Benoit, L., Sensiau, C., and Poinsot, T., 2007. "Acoustic Modes in Combustors with Complex Impedances and Multidimensional Active Flames". *AIAA Journal,* ***45***(2), pp. 426–441.

[31] Krüger, U., Hüren, J., Hoffmann, S., Krebs, W., and Bohn, D., 1999. "Prediction of Thermoacoustic Instabilities With Focus on the Dynamic Flame Behavior for the 3A-Series Gas Turbine of Siemens KWU". In Volume 2: Coal, Biomass and Alternative Fuels; Combustion and Fuels; Oil and Gas Applications; Cycle Innovations, ASME 99-GT-111, American Society of Mechanical Engineers, p. V002T02A016.

[32] Evesque, S., and Polifke, W., 2002. "Low-Order Acoustic Modelling for Annular Combustors: Validation and Inclusion of Modal Coupling". In Volume 1: Turbo Expo 2002, ASME GT-2002-30064, ASMEDC, pp. 321–331.

[33] Parmentier, J.-F., Salas, P., Wolf, P., Staffelbach, G., Nicoud, F., and Poinsot, T., 2012. "A simple analytical model to study and control azimuthal instabilities in annular combustion chambers". *Combustion and Flame,* ***159***(7), July, pp. 2374–2387.

[34] Bauerheim, M., Parmentier, J.-F., Salas, P., Nicoud, F., and Poinsot, T., 2014. "An analytical model for azimuthal thermoacoustic modes in an annular chamber fed by an annular plenum". *Combustion and Flame,* ***161***(5), May, pp. 1374–1389.

[35] Yang, D., Laera, D., and Morgans, A. S., 2019. "A systematic study of nonlinear coupling of thermoacoustic modes in annular combustors". *Journal of Sound and Vibration,* ***456***, Sept., pp. 137–161.

[36] Bloch, F., 1929. "Über die Quantenmechanik der Elektronen in Kristallgittern". *Zeitschrift für Physik,* ***52***(7-8), July, pp. 555–600.

[37] Mensah, G. A., Campa, G., and Moeck, J. P., 2016. "Efficient Computation of Thermoacoustic Modes in Industrial Annular Combustion Chambers Based on Bloch-Wave Theory". *Journal of Engineering for Gas Turbines and Power,* ***138***(8), Aug., p. 081502.

[38] Ghirardo, G., Di Giovine, C., Moeck, J. P., and Bothien, M. R., 2019. "Thermoacoustics of Can-Annular Combustors". *Journal of Engineering for Gas Turbines and Power,* ***141***(1), Jan., p. 011007.

[39] Haeringer, M., and Polifke, W., 2019. "Time Domain Bloch Boundary Conditions for Efficient Simulation of Thermoacoustic Limit-Cycles in (Can-)Annular Combustors". *Journal of Engineering for Gas Turbines and Power,* ***141***(12), p. 121005.

[40] Poinsot, T., and Veynante, D., 2012. *Theoretical and Numerical Combustion*, 3 ed. CNRS, Paris.

[41] Schuller, T., Durox, D., Palies, P., and Candel, S., 2012. "Acoustic decoupling of longitudinal modes in generic combustion systems". *Combustion and Flame,* ***159***(5), May, pp. 1921–1931.

[42] Marble, F. E., and Candel, S. M., 1977. "Acoustic Disturbance from Gas Non-Uniformities Convected Through a Nozzle". *Journal of Sound and Vibration,* ***55***(2), Nov., pp. 225–243.

[43] Bauerheim, M., Duran, I., Livebardon, T., Wang, G., Moreau, S., and Poinsot, T., 2016. "Transmission and reflection of acoustic and entropy waves through a stator–rotor stage". *Journal of Sound and Vibration,* ***374***, pp. 260–278.

[44] Morgans, A. S., and Duran, I., 2016. "Entropy Noise: A Review of Theory, Progress and Challenges". *International Journal of Spray and Combustion Dynamics,* ***8***(4), pp. 285–298.

[45] Chu, B.-T., 1953. "On the generation of pressure waves at a plane flame front". *Symposium (International) on Combustion,* ***4***(1), Jan., pp. 603–612.

[46] Crocco, L., 1951. "Aspects of Combustion Stability in Liquid Propellant Rocket Motors Part1: Fundamentals. Low frequency instability with monopropellants". *Journal of the American Rocket Society,* ***21***(6), pp. 163–178.

[47] Bauerheim, M., Cazalens, M., and Poinsot, T., 2015. "A theoretical study of mean azimuthal flow and asymmetry effects on thermo-acoustic modes in annular combustors". *Proceedings of the Combustion Institute,* ***35***(3), pp. 3219–3227.

[48] Haeringer, M., Fournier, G. J. J., Meindl, M., and Polifke, W., 2020. "A Strategy to Tune Acoustic Terminations of Single-Can Test-Rigs to Mimic Thermoacoustic Behavior of a Full Engine". In ASME Turbo Expo 2020: Turbomachinery Technical Conference & Exposition.

[49] Emmert, T., 2016. "State Space Modeling of Thermoacoustic Systems with Application to Intrinsic Feedback". Ph.D. Thesis, TU München, München, Germany.

[50] Emmert, T., Meindl, M., Jaensch, S., and Polifke, W., 2016. "Linear State Space Interconnect Modeling of Acoustic Systems". *Acta Acustica united with Acustica,* ***102***(5), pp. 824–833.

[51] Mensah, G. A., 2019. "Efficient computation of thermoacoustic modes". PhD thesis, Technische Universität Berlin.

APPENDIX: DERIVATION OF T-JUNCTION MODEL

The derivation does not show any major difficulties but requires some mathematical precautions. Eqn. (8) has 6 unknowns for only 3 equations. The unknown g_A can be easily eliminated by inserting Eqn. (9) in Eqn. (8):

$$\begin{cases} f_C + g_C = f_B + g_B & \text{(20a)} \\ f_C - g_C = f_B - g_B + \alpha f_A (1 - \mathscr{R}_m) & \text{(20b)} \end{cases}$$

Combining Eqn. (10, 11) allows us to directly connect locations B and C of the T-junction.

$$\begin{bmatrix} f_C \\ g_C \end{bmatrix} = \begin{bmatrix} e^{i\left(\frac{2\pi m}{N} + kL\right)} & 0 \\ 0 & e^{i\left(\frac{2\pi m}{N} - kL\right)} \end{bmatrix} \begin{bmatrix} f_B \\ g_B \end{bmatrix} \tag{21}$$

With Eqn. (21), Eqn. (20) simply becomes:

$$\begin{cases} e^{i\left(\frac{2\pi m}{N}+kL\right)} f_B + e^{i\left(\frac{2\pi m}{N}-kL\right)} g_B = f_B + g_B & \text{(22a)} \\ e^{i\left(\frac{2\pi m}{N}+kL\right)} f_B - e^{i\left(\frac{2\pi m}{N}-kL\right)} g_B = f_B - g_B + \alpha f_A (1-\mathscr{R}_m) & \text{(22b)} \end{cases}$$

which is a system of 2 equations for 3 unknowns. But the unknown f_A can be expressed as a function of f_B and g_B using Eqn. (8a)

$$f_A = \frac{f_B + g_B}{1+\mathscr{R}_m} \tag{23}$$

This requires the reflection not to be $\mathscr{R}_m = -1$ but this is a meaningful hypothesis for this configuration. Indeed if the reflection coefficient is $\mathscr{R}_m = -1$, Eqn. (8a) leads to:

$$\begin{cases} f_B = -g_B & \text{(24a)} \\ f_C = -g_C & \text{(24b)} \end{cases}$$

Inserting Eqn. (21, 24b) into Eqn. (24a) writes

$$f_C e^{i\frac{2\pi m}{N}} \left(e^{ikL} - e^{-ikL}\right) = 0 \tag{25}$$

Equation (25) is satisfied for one of the following conditions:

- $f_C = 0$. This implies $f_A = g_A = f_B = g_B = g_C = f_C = 0$, which is the trivial case where no acoustics is present in the system.
- $\left(e^{ikL} - e^{-ikL}\right) = 0$. The frequency is then imposed by the condition

$$kL = \text{He} = h\pi, \quad h \in \mathbb{N} \tag{26}$$

The equivalent reflection coefficient $\mathscr{R}_m$ can be equal to -1 only if Eqn. (26) is satisfied. Because of the periodicity of the complex exponential, we can limit the study to only 2 cases: $\mathrm{He} = 0$ and $\mathrm{He} = \pi$.

We consider the first case where $\mathrm{He} = 0$. Equation (22a) simply becomes

$$\left(e^{i\frac{2\pi m}{N}} - 1\right)(f_B + g_B) = 0 \tag{27}$$

Equation (27) is satisfied for the following conditions:

- $m = 0$. Inserting this condition into Eqn. (22b) leads to the only non trivial solution $\mathscr{R}_0(\mathrm{He} = 0) = 1$
- if $m \neq 0$, we have the condition $f_B + g_B = 0 = f_A + g_A$ which directly reads to $\mathscr{R}_m(\mathrm{He} = 0) = -1$

We now consider the second case where $\mathrm{He} = \pi$. Equation (22a) becomes

$$\left(e^{i\frac{2\pi m}{N}} + 1\right)(f_B + g_B) = 0 \tag{28}$$

Equation (28) is satisfied for the following conditions:

- $m = N/2$. Inserting this condition into Eqn. (22b) leads to the only non trivial solution $\mathscr{R}_{N/2}(\mathrm{He} = \pi) = 1$
- if $m \neq N/2$, we have the condition $f_B + g_B = 0 = f_A + g_A$ which directly reads to $\mathscr{R}_m(\mathrm{He} = \pi) = -1$

The equivalent reflection coefficient $\mathscr{R}_m$ takes the value -1 only at frequency $\mathrm{He} = 0$ for all azimuthal orders, except the axial mode, and at frequency $\mathrm{He} = \pi$ for all azimuthal orders, except the push-pull mode. Otherwise, for every other frequency, $\mathscr{R}_m \neq -1$. Inserting Eqn. (23) in Eqn. (22) allows us to eliminate the unknown f_A and have a final system of 2 equations with 2 unknowns whose final form is Eqn. (13).